CrystEngComm

ARTICLE

Solid state halogen bonded networks vs. dynamic assemblies in solution: explaining N···X interactions of multivalent building blocks

Tiia-Riikka Tero,[a] Kirsi Salorinne,[a] Sami Malola,[b] Hannu Häkkinen[a,b] and Maija Nissinen*[a]

Tetrapyridine functionalized resorcinarene macrocycles were used as multivalent building blocks for the construction of halogen bonded networks with aryl halide linkers. In the solid state, resorcinarene macrocycles and aryl halide linker molecules assembled into interpenetrated, multidimensional halogen bonded networks with porous structure caused by the 3D block scaffold of the resorcinarenes. ^{19}F NMR spectroscopy proved halogen bond formation also in solution, as either upfield or downfield shifts were observed depending on the bivalent or monovalent halogen bond binding mode. The binding mode in solution was explained by density functional theory computations.

Introduction

In recent years one of the compelling interactions in supramolecular chemistry has been halogen bonding (XB),[1] which is a noncovalent interaction between an electrophilic halogen atom and a Lewis base.[2] Particularly, the directionality and predictability of halogen bonds[3] have already achieved considerable attention in the construction of, for example, magnetic materials[4] and liquid crystals,[5] as well as other types of solid state networks. The simplest networks consist of linear building blocks,[6] but also more complex and multidimensional building blocks having several XB binding sites are known. Examples of more complicated structures include branched tectons[7] macrocyclic porphyrin structures,[8] piperazine cyclophanes[9] and bis-urea macrocycles[10] to mention a few.

One attractive approach to construct more diverse and multidimensional halogen bonded networks is to use a well-known group of concave macrocycles, namely calixarenes or closely related resorcinarene,[11] as three-dimensional preorganized scaffolds. Previously, the macrocyclic cavity and halogen bonding interactions have mainly been utilized in guest binding[12] – with a handful of examples reporting a capsular and deep cavity cavitand-like halogen bonded assemblies.[13] The *boat* conformation of resorcinarenes, in particular, has shown to be extremely versatile in the construction of multidimensional hydrogen bonded networks.[14] The well-defined and preorganized macrocyclic structure provides intrinsic dimensionality and order to the network assembly.

Majority of the research of the halogen bonded assemblies has focused solely on the solid state structures, but understanding the properties and behavior of halogen bonding in solution has recently gained increasing interest.[15] To a great extent, NMR spectroscopy has proven to be a convenient and informative tool to study halogen bonding in solution.[6b,15,16] For smaller halogen bond systems even association constants reflecting the strength of the interaction have been determined.[15,16] Profound discussion of halogen bond formation and properties of multivalent XB donors and acceptors in solution, however, are still lacking, and phenomena, such as hierarchy, the number of halogen bonds formed in the multivalent systems (fully vs partially XB bonded) and the comparison to binding behavior in solid state structures, are still scarcely explained and poorly understood. Only recently, Jungbauer et al.[17] reported strong molecular recognition of a finite three-point halogen bonded assembly both in solution and in the solid state, where the receptor/substrate match was nearly perfect when the number of the donor and acceptor sites was equal but less optimal with substrates having fewer acceptor sites than the ideal three.

Our earlier study explaining the properties of halogenated resorcinarenes and their solid state packing that was driven by intermolecular halogen bonds[18] intrigued us to explore the potential of tetrapyridine functionalized resorcinarenes in the construction of halogen bonded networks with aryl halides as connecting linkers. Herein, we present the synthesis and solution dynamics of two multidimensional resorcinarene based halogen bond acceptors, as well as, a successful construction of two network structures stabilized by halogen bonds, in which the dimensionality and architecture was obtained by the resorcinarene core, directionality by the

[a.] Department of Chemistry, Nanoscience Center, University of Jyvaskyla, P.O. Box 35, FI-40014 Jyvaskyla, Finland. E-mail: maija.nissinen@jyu.fi
[b.] Department of Physics, Nanoscience Center, University of Jyvaskyla, P.O. Box 35, FI-40014 Jyvaskyla, Finland
† Electronic Supplementary Information (ESI) available: Detailed experimental procedures, spectroscopic and crystallographic data, computational data, and additional figures are provided. See DOI: 10.1039/x0xx00000x

a)

1: X=N, 3-pyridyl
2: X=N, 4-pyridyl
3: X=C, benzyl

boat₁ ⇌ *boat₂*

b)

A **B** **C**

D **E**
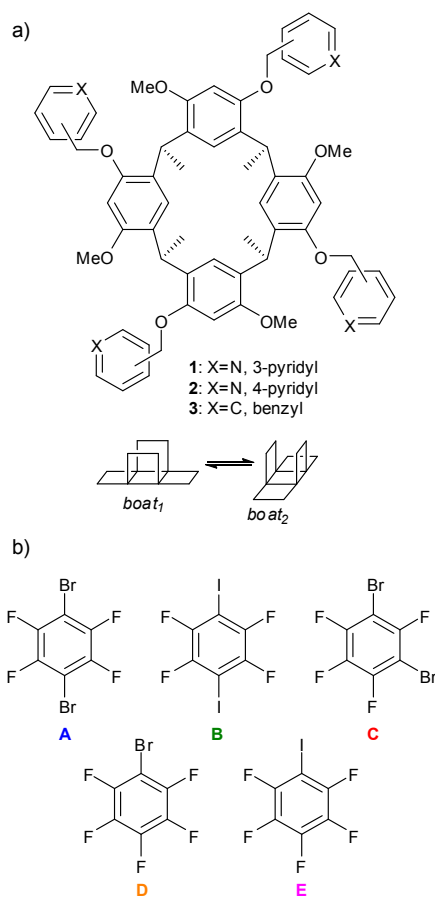
Fig. 1 (a) Chemical structure of the pyridine functionalized resorcinarene based tetravalent halogen bond acceptors **1** and **2**, and the reference compound **3**. Schematic presentation of the boat1-boat2 interconversion is shown below. (b) Structures of the halogen bond donors: 1,4-dibromo- (**A**), 1,4-diiodo- (**B**), and 1,3-dibromotetrafluorobenzene (**C**); bromo- (**D**) and iodopentafluorobenzene (**E**).

podand pyridine arms and cohesion by the aryl halide linkers. Solution behavior of the halogen bond donor-acceptor systems were additionally investigated in detail using NMR spectroscopic techniques and the challenges imposed by the multiple XB sites, such as several possible simultaneous interactions in solution, were resolved by computational methods using density functional theory (DFT) that provided important insight into the changes observed in the ^{19}F NMR spectra and into the behavior of these complex systems in solution.

Results and discussion

Design and structural properties of the halogen bond acceptors 1 and 2

In order to form multidimensional halogen bonded networks expanding to four different directions, C-methyl tetramethoxy resorcinarene was selected as a platform and pyridine podand arms as the halogen bond accepting substituents on the upper rim (Fig. 1a). Since halogen bonds are highly directional and linear in nature,[3] two different constitutional isomers of

tetravalent halogen bond acceptors differing only by the position of the nitrogen atom in the pyridine rings (3- or 4-pyridyl; **1** and **2**, respectively) were synthesized to control the node angles of the networks. The choice of the well-defined *C*-methyl tetramethoxy resorcinarene[19] as a platform minimized the unwanted influence of the longer lower rim alkyl chains[20] on the crystal packing and on the network assembly.

The pyridine functionalized tetramethoxy resorcinarenes **1** and **2** were synthesized using a similar protocol as reported earlier for pyridine functionalized resorcinarenes by McIldowie et al.[21] resulting in the desired resorcinarene derivatives **1** and **2** with 47–49% yields. Full structural characterization was done by NMR spectroscopy, high-resolution mass spectrometry and X-ray crystallography.

As expected, tetrapyridine functionalized *C*-methyl tetramethoxy resorcinarenes **1** and **2** adopt a *boat* conformation both in solution and in the solid state as a result of the lack of *crown* conformation stabilizing intramolecular upper rim hydrogen bonds. In solution, the *boat* conformation usually interconverts between *boat₁* and *boat₂* conformers (Fig. 1a) but the conversion is typically too fast to be observed on the NMR time scale at 30 °C, and the proton signals appear as one sharp and averaged set of signals instead of the expected two for the C_{2v} symmetrical *boat* conformation.[22] The pyridine functionalized resorcinarenes **1** and **2**, however, showed slower dynamic properties than anticipated, which was seen as very broad proton signals at 30 °C (Fig. 2). Therefore, variable temperature NMR measurements in deuterated chloroform starting at 30 °C and decreasing in 10 degree decrements to -30 °C were done in order to investigate the unexpected dynamic behavior in more detail. At -30 °C the proton spectra of the resorcinarene derivatives **1** and **2** indeed showed two sets of very sharp signals consistent with the C_{2v} symmetry of the *boat* conformation.

Possible reasons for the unusually slow *boat*-to-*boat* interconversion were reasoned to be either the interaction of the pyridine substituents with solvent or the effect of the short lower rim alkyl chain length on the interconversion dynamics. To explore the possible solvent effects on the dynamic properties, a proton spectrum of the benzyl analogue **3**[23] without Lewis basic pyridine nitrogens was recorded for comparison. The reference compound **3** showed the same

a)

b)
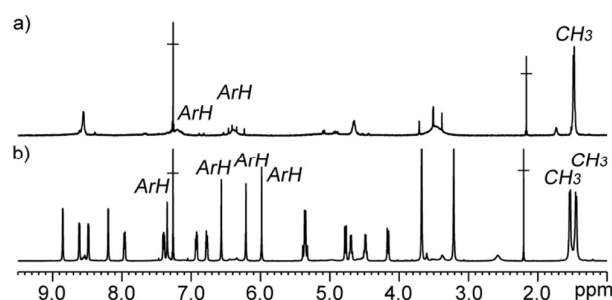
Fig. 2 ^{1}H NMR spectra of the tetrapyridine functionalized C-methyl tetramethoxy resorcinarene **1** in CDCl₃ at 30 °C (a) and at -30 °C (b). Aromatic and lower rim methyl protons are assigned.

broadening of the proton signals at 30 °C, which proved that intermolecular interactions between pyridine nitrogen and solvent played no role in dynamics leaving the flexibility of the macrocyclic ring caused by the short lower rim alkyl chains as a possible reason. This reasoning is also supported by the earlier reported resorcinarene tetrapodand derivatives[18,21] with longer alkyl chains, as well as the ethyl analogue[23] of the reference compound, which all showed sharp proton NMR signals at 30 °C. The literature examples of the rare scoop,[24] chair[25] and diamond[26] conformers observed for the *C*-methyl resorcinarene also indicate the conformational flexibility of the resorcinarene core. Therefore, it appears that larger substituents at the lower rim restrict the conformational mobility of the resorcinarene core more, whereas the smaller methyl groups allow extended movement thus slowing down the interconversion rate.

Further evidence of the conformational mobility was provided by the crystal structures of the pyridine functionalized resorcinarene derivatives **1** and **2**, which crystallized as four different solvate structures from chloroform (**2**-CHCl3) solution or from chloroform-methanol (**1**-MeOH), chloroform-acetonitrile (**2**-MeCN) and chloroform-ethanol (**2**-EtOH) mixtures of the respective resorcinarene derivatives (see crystallization details in ESI). In all of these structures, the resorcinarene skeleton adopts a *boat* conformation and in three of them (**1**-MeOH, **2**-MeCN, and **2**-EtOH) the horizontal aromatic rings are bent over the plane formed by the methine bridges (183.9-187.7°). This overbending might be the cause for the slower *boat*-to-*boat* interconversion of resorcinarenes **1** and **2** in solution at higher temperature as seen by the broadened NMR signals.
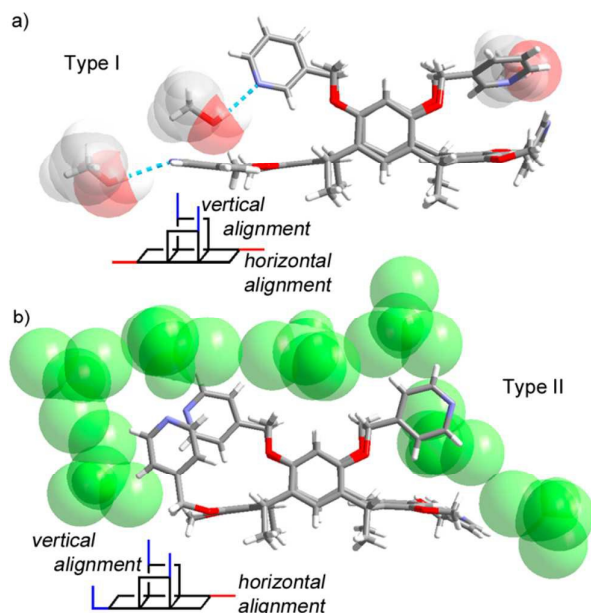
Fig. 3 The *boat* conformations of **1** and **2** in the solid state. The two orientation trends of the pyridine arms, type I and II, are shown for the structures **1**-MeOH (a) and **2**-CHCl₃ (b), and presented schematically below the structures. Hydrogen bonded and surrounding solvent molecules are presented as space fill models.

The crystal structures also confirmed the ability of the pyridine functionalized resorcinarene tetrapodands **1** and **2** to function as potential multidimensional halogen bond acceptors, which was seen in the orientation and weak interactions of the pyridine rings with the solvent molecules. Depending on the surrounding interactions or the lack of them the podand arms showed a clear tendency to orient in certain directions. The pyridine arm can settle according to the plane formed by its parent aromatic ring (*anti*-orientation, *Ar**C**-O-**CH**₂-Py**C***) or perpendicular to the plane (*gauche*-orientation, Table S1). In the structures **1**-MeOH and **2**-EtOH the arms are hydrogen bonded to the solvent molecules and they all orient to the same direction as their parent aromatic ring (*anti*) expanding the cavity dimensions to the full, both vertically and horizontally (Type I, Fig. 3a and Fig. S12). On the other hand, without any solvent interactions present (structures **2**-MeCN and **2**-CHCl₃), one of the pyridine arms attached to the horizontal aromatic ring orients along the vertical plane (*gauche*) blocking the expansion of the cavity dimensions from that end (Type II, Fig. 3 and Fig. S13). This indicates that the *anti*-orientation is induced by the solvent coordination. The same two trends were also seen in earlier structures of pyridine functionalized resorcinarenes.[18,21] In all structures of compounds **1** and **2**, regardless of the 3- or 4-position, the pyridine nitrogen atoms point away from the cavity being properly aligned for forming intermolecular interactions.
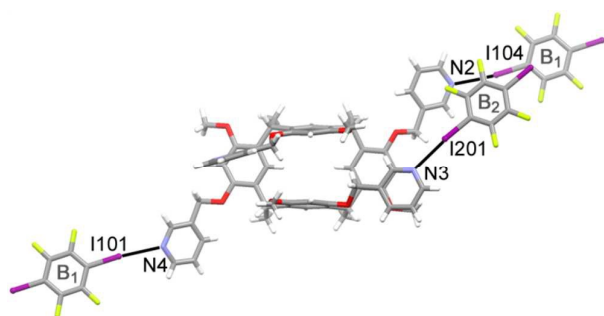
Halogen bonding

In order to achieve multidimensional halogen bonded networks, three different bivalent halogen bond donors with either linear 180° angle (**A** and **B**) or 120° angle (**C**) between the donor sites were selected as the linker molecules (Fig. 1b). Aryl halides suit well for the network formation because they are structurally rigid and not too elongated to impede the close packing in the solid state. Since the bivalent linkers **A**-**C** are able to form interactions from either one or two donor sites, two monovalent linkers (**D** and **E**, Fig. 1b) were additionally selected as reference due to their unambiguous interactions.

Solid state networks. The study was started with crystallization experiments of tetravalent resorcinarenes **1** and **2** with the linkers **A**-**E**. So far only the crystallizations with the strongest halogen bond donor, namely linear bivalent iodo linker **B**, gave suitable crystals for crystallographic studies, affording a linear chain structure of the 3-pyridine functionalized resorcinarene **1** and a tangled grid structure of the 4-pyridine functionalized resorcinarene **2**. In both of the structures, the resorcinarene core adopts a *boat* conformation and the torsion angles (*Ar**C**-O-**CH**₂-Py**C***) of the pyridine arms are *anti*-oriented i.e. type I (**Fig. 3**a), and the pyridine rings are horizontally aligned. As such, the halogen bonds are aligned 2-dimensionally but with respect to the resorcinarene platform, the bivalent linker **B** can interconnect via halogen bond interactions between the neighboring resorcinarene at two or more levels creating multidimensional nanostructures, which are discussed in more detail below.
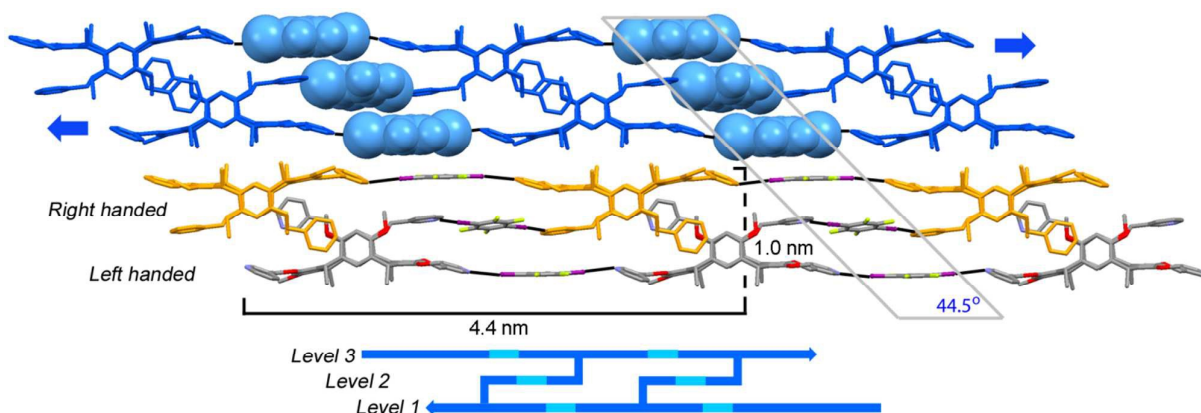
Fig. 4 Crystal packing of structure **1**-**B** and a schematic presentation of halogen bonding chains (below). The single chain formed by the resorcinarenes of the same inherent chirality is shown in elemental colors and its enantiomeric pair in the same double chain in orange. The next double chain piled on top is shown in blue (linkers shown as a space fill model). The "leaning tower" formed by the stacked linker molecules is highlighted by a grey parallelogram. Halogen bonds are shown as black lines and hydrogen atoms have been omitted for clarity.


Fig. 5 Halogen bonds (black lines) formed by the resorcinarene **1** with 1,4-diiodotetrafluorobenzene **B** in structure **1**-**B**. Halogen bonding nitrogen and iodine atoms are labeled.

Resorcinarene **1** and linker **B** crystallized from a chloroform solution in a resorcinarene:linker ratio of 2:3 (**1**-**B**, **Fig. 4**). Three of the pyridine arms (N2, N3, N4, **Fig. 5**) form halogen bonds with linker **B** molecules, one at the upper rim level and two at the level of the methine bridges, whereas the fourth pyridine ring (N1) on the level of the upper rim is engaged in forming π-π stacking interactions (3.97 Å) with the neighboring resorcinarenes. Linker **B$_1$** connects the resorcinarenes of the same inherent chirality[27] into continuous chains as the linker molecule forms halogen bonds from both of its halogen bond donor sites (N2···I104 = 2.89 Å/172.9° and N4···I101 = 2.86 Å/174.3°; **Fig. 4**, elemental color). Pyridine arm N3 and the second linker **B$_2$** form a similar halogen bond (N3···I201 = 2.87 Å/173.9°) between two resorcinarenes of the different inherent chirality and connect the opposite facing single chains into a double chain consisting of 4.4×1.0 nm loops with three successive halogen bonded layers (**Fig. 4**, orange and elemental color). The double chains are then piled on top of each other and the two crystallographically independent linker molecules stack diagonally in a 44.5° angle resembling a structure of a "leaning tower" (**Fig. 4**, blue). The piled double chains are horizontally packed side by side via the fourth pyridine arm (N1) with chloroform molecules filling the voids in between (Fig. S14).

Resorcinarene **2** forms a 2:4 (resorcinarene:linker) network with the linker **B** when crystallized from a mixture of chloroform-methanol (structure **2**-**B**). The structure is highly symmetrical showing only a half of the resorcinarene **2** and one linker molecule **B** in an asymmetric unit. Unlike in any of the other structures (**2**-MeCN, **2**-CHCl$_3$, **1**-MeOH, **2**-EtOH and **1**-**B**) the *boat* conformation of the resorcinarene skeleton is highly twisted[28] causing a curved shape to the macrocycle core (Fig. S11). The repeating unit in this network structure, the grid mesh, is composed of four linker **B** molecules adjoining four resorcinarene **2** molecules at the nodes via N1···I104 (2.81 Å, 178.4°) and N2···I102 (2.82 Å, 175.6°) halogen bonds (mesh area 7.4 nm^2, **Fig. 6**). All four pyridine arms are horizontally aligned at two different levels, similarly to resorcinarene derivative **1** in structure **1**-**B**. This, together with the highly twisted and curved resorcinarene core, enables meshes of three consecutive individual grids (**Fig. 6**c: red, blue and orange) to go under and over each other thus forming an interpenetrated structure, where the crossing points of the grids are held together by a linker-pyridine π-π stacking interaction (3.65 Å). Each tangled grid layer is composed of resorcinarene molecules with the same inherent chirality. The layers are stacked diagonally on top of one another alternating with the inherent chirality of resorcinarenes (Fig. S15). The stacked layers form porous channels filled with chloroform molecules (cross-section area 64 Å^2, **Fig. 7**). Thus, unlike in structure **1**-**B**, where the different inherently chiral resorcinarenes are part of the same structural entity, in structure **2**-**B**, the self-assembly shows enantiomeric separation.

These two network structures show that the pyridine functionalized resorcinarenes **1** and **2** have an ideal geometry to form multilevel 2-dimensional frameworks with the linear bivalent linker molecules in the solid state, which is mainly due to the halogen bond accepting pyridine arms that settle into different levels provided by the resorcinarene cavity in the boat conformation. The rigidity and concave shape of the resorcinarene core combined with the planar linkers furthermore enable the formation of porous structures as seen by the solvent filled interstice. In addition, varying the position of the pyridine nitrogen atoms controls the direction of the
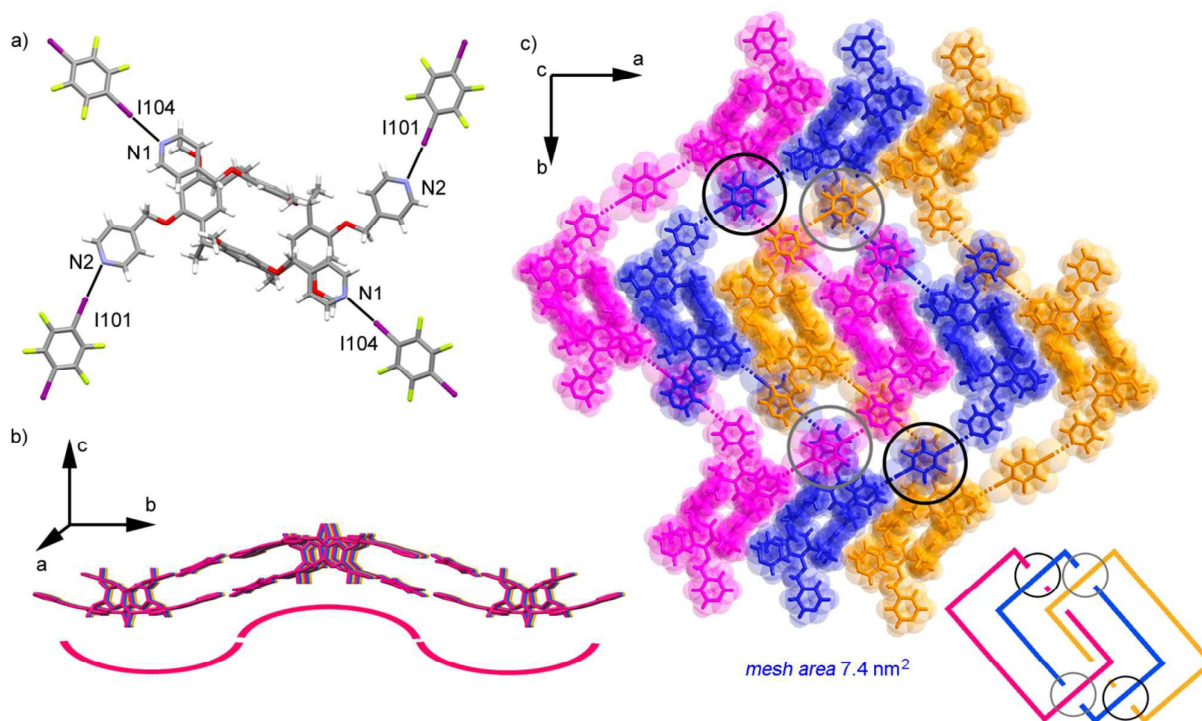
Fig. 6 Halogen bonds formed by resorcinarene **2** linker **B** in the structure **2-B** (a), nitrogen and iodine atoms are labeled and halogen bonds are shown in black. Crystal packing viewed along a- (b) and c-axes (c). The three repeating grids on the tangled layer are shown in red, blue and orange. The points where the blue grid goes under (grey) and over (black) the adjacent grids are circled and also presented in the schematic presentation. Hydrogen atoms (b, c) have been omitted for clarity.
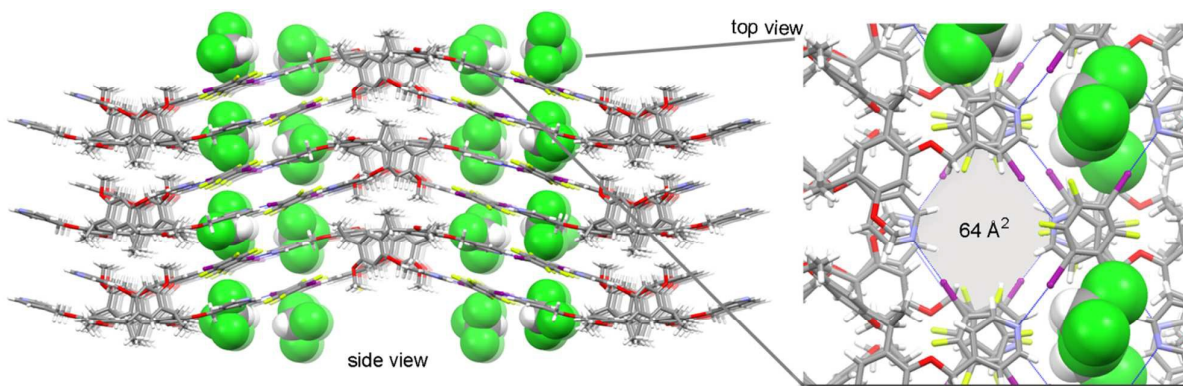

Fig. 7 Side and top views of the porous channels filled with chloroform molecules in the structure **2-B**. Chloroforms are shown as space fill models and in the top view chloroforms are omitted from one channel showing the cross-section area highlighted in grey.

network expansion: When the nitrogen atom is at the 3-position the network builds linearly to two directions, whereas nitrogen at the 4-position expands the network to all four directions.

Dynamic solution assemblies. In addition to the explicit solid state networks, the solution behavior between the tetravalent resorcinarenes **1** and **2** and the bi- and monovalent linkers **A**−**E** in terms of halogen bonding were complemented by means of ^{1}H, ^{19}F and diffusion ordered (DOSY) NMR spectroscopy. Deuterated chloroform was used as a solvent because of the poor solubility of resorcinarenes **1** and **2** in other solvents. In solution there are a multitude of different possible interactions between resorcinarenes (R), linkers (L) and the

surrounding solvent molecules (S). Thus, in addition to halogen bonding, also hydrogen bonding and halogen-halogen interactions have to be taken into consideration (**Fig. 8**).

^{19}F NMR spectroscopy is ideal for studying the interactions of the aryl halide linkers as the changes in the chemical shifts of the linker molecules can be followed directly, and the information is also conveyed about the nature and the strength of the interaction. Therefore, in order to study halogen bonding between resorcinarenes **1**–**2** and the linker molecules **A**–**E**, samples with different concentrations of the interacting species (1:0 to 1:1) were prepared and the chemical shift differences then compared with the signals of the pure linker molecule. It was contemplated that increasing
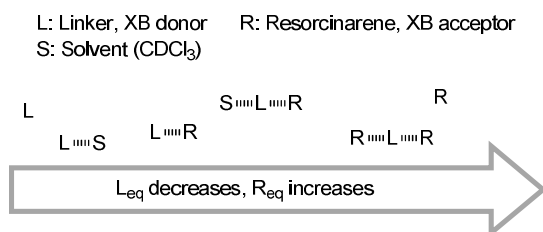
Fig. 8 Schematic presentation of the possible interactions of the resorcinarenes **1**–**2** and linkers **A**–**E** in deuterated chloroform. Interactions are depicted as black dashed lines and the arrow shows the change in molarity of the interacting species.

the equivalency of the halogen bond accepting resorcinarenes the probability for halogen bond formation will also increase.

With monovalent linkers **D** and **E** increasing the concentration of the halogen bond acceptor resorcinarenes **1** and **2** showed a downfield shift of the linker fluorine signals up to 1:1 mixtures, consistent to the previously reported literature[16c] (**Fig. 9**a and S16-19). The iodo linker **E** showed a much larger downfield shift (up to 0.15 ppm) than the bromo linker **D**, which showed only a minimal shift of 0.01 ppm. The bivalent *meta*-substituted linker **C** showed similar changes in the chemical shifts to the monovalent linkers **E** and **D** (**Fig. 9**d): increasing the resorcinarene concentration caused a downfield shift (avg. 0.01-0.04 ppm), and at 1:1 mixtures the shift became more significant (avg. 0.11 ppm). In the case of the bivalent linear *para*-substituted linkers **A** and **B**, increasing the resorcinarene concentration caused at first a downfield shift of the fluorine signals (0.02-0.05 ppm, **Fig. 9**b-c), but when the concentration of resorcinarene was increased up to 1:1 ratio the fluorine signals shifted dramatically upfield (-0.21 ppm for **A** and -0.03 ppm for **B**, **Fig. 9**b and c). Contrary to monolinkers **D** and **E**, the largest changes in the fluorine shifts were observed with the bromo linker **A** (0.21 ppm) instead of the linker **B** with iodo atoms as XB donors (0.03 ppm).

In order to explore the reasons behind the bivalent linkers **A** and **B** showing both downfield and upfield shifts in the ^{19}F NMR studies, DFT calculations of the model systems composed of halogen bond donating linkers **A** and **B**, halogen bond accepting pyridine ring and solvent chloroform were performed (Fig. S24, Table S3). As a starting point the relative ^{19}F NMR shift of the fluorine atoms of the different interactions summarized in Fig. 8 were calculated (**Fig. 10**). In 1:0 mixture (L:R) the possible prevailing interaction of the linkers in solution is hydrogen bonds (HB) with the solvent, and thus the signal of a linker is most likely an average of these interactions (L···S). The linker has the total of four fluorine atoms meaning that in theory each linker could form four HBs. Therefore, ^{19}F NMR shifts were calculated for combinations of pure L, L+S, L+2S and L+4S which shows a shift trend toward upfield, respectively. The upward shift takes also place in experimental measurements since the chemical shifts of linkers **A** and **B** in noncoordinating solvent, pentane, are downfield (-132.89 ppm for **A** and -119.44 ppm for **B**)[16b] compared to the chemical shifts in deuterated chloroform (-134.48 ppm for **A** and -121.20 ppm for **B**).
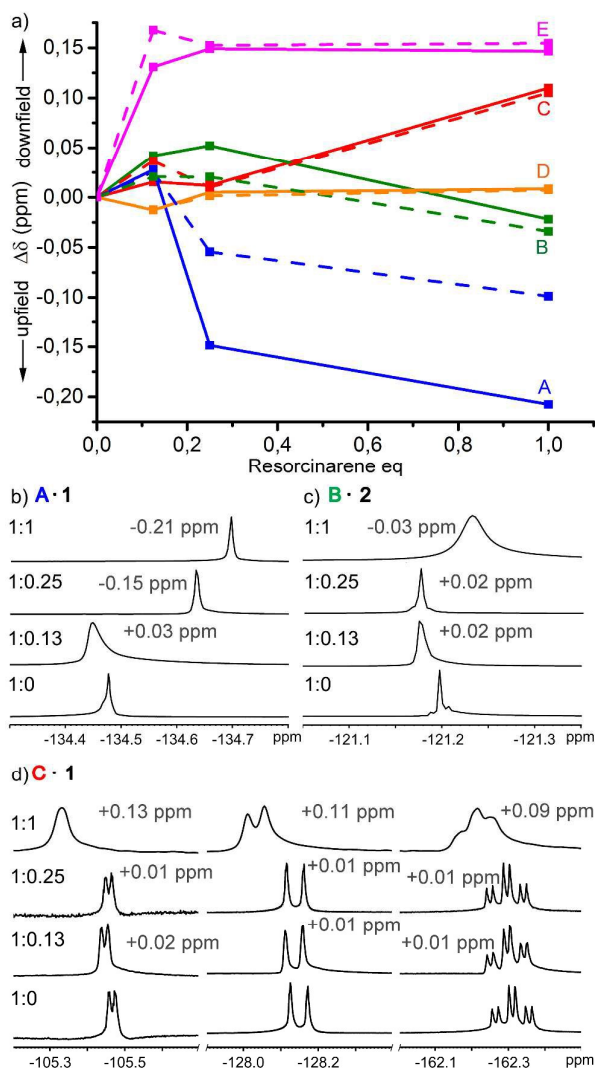
Fig. 9 Graphical presentation of the ^{19}F NMR chemical shift changes (ppm) of linkers **A**-**E** (blue, green, red, orange, magenta) with increasing concentration of resorcinarenes **1** (solid line) and **2** (dash line). For linkers **C**-**E** the average shift of the three unequal fluorine signals is shown. (b-d) Representative ^{19}F NMR spectra of the bivalent linkers **A** (b), **B** (c) and **C** (d) with either resorcinarenes **1** or **2** at 30 °C showing the fluorine chemical shift changes at different linker:resorcinarene concentrations. The signal shifts (ppm) are compared to the signals of the pure linkers (1:0, bottom spectra).

When a halogen bond acceptor, pyridine, is added to the model system, the linker **A** (L···R) shows a downfield shift compared to the average L+S shift. With the linker **B**, however, the signal shifts slightly upfield, but it is downfield compared to L+4S signal. When the concentration of the bivalent *para* linkers **A** and **B** is decreased, the probability of forming two halogen bonds from the opposite XB donor sites (R···L···R) becomes the prevailing type of interaction instead of single halogen bonds. In the presence of the double halogen bonding, the calculated signals of the linkers clearly shift upfield. Therefore, with a large excess of halogen bond donating linkers, it is more likely
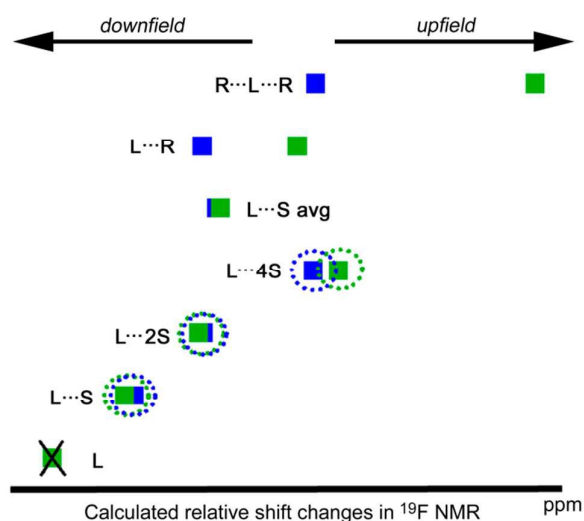
Fig. 10 Schematic presentation of the calculated relative shift changes of fluorine signals in ^{19}F NMR due to the prevailing dominating interactions of linkers **A** (blue) and **B** (green) with solvent molecules and with pyridine ring of resorcinarene. The pure linker is left out since it is not observed in solution NMR experiments. L = linker (XB donor), R = resorcinarene (XB acceptor) and S = solvent (CHCl₃).

that only a single halogen bond forms in solution, which is seen as a downfield shift of the fluorine signals. When the halogen bond acceptor concentration exceeds the available donor sites, the probability of double halogen bonding to the bivalent linker molecule increases, which would explain the experimentally observed upfield shift of the fluorine signal upon the increased concentration of resorcinarene (1:1). An intriguing observation is that the bivalent *meta*-linker **C** seems to behave similarly to the monovalent linkers **D** and **E**, as observed by downfield shifts of the fluorine signals in the NMR spectrum. This suggests that the angle of the *meta*-substitution is not ideal for double halogen bonding to the neighboring resorcinarene derivatives.

The shapes of the fluorine NMR signals are much broader for linker **B** than for linker **A**, which could indicate that there are more simultaneous, and competing interactions between the iodo linker **B** and resorcinarene acceptors and solvent molecules. Therefore, the halogen bonding process could be more dynamic in nature than that of the bromo linker **A**. The sharper fluorine signals of the bromo linker **A** at higher resorcinarene concentrations, on the other hand, indicate most likely that the system reaches equilibrium faster and majority of the linker molecules are double halogen bonded.

^{1}H NMR measurements, which disclose the information of the halogen bonding interaction with respect to the halogen bond accepting resorcinarenes, were done at -30 °C because of the dynamic behavior of the resorcinarene macrocycle broadening the proton signals at higher temperatures. In the proton spectra the changes in the chemical shifts of the pyridine arms of resorcinarenes **1**-**2** in the presence of linkers **A**-**E** were not as significant as the shifts in the fluorine spectra, but the changes were nonetheless distinguishable (0.01-0.05 ppm Fig. S23). Due to the C_{2v} symmetry of the *boat* conformation two sets of signals of the pyridine arms are

visible corresponding to the pyridine podand arms attached to either on the horizontal or vertical aromatic rings. Only one set of signals was affected upon halogen bonding suggesting that the tetravalent resorcinarenes **1** and **2** do not form more than two halogen bonds in solution unlike in the solid state, where three or all four halogen bond accepting sites were occupied.

In order to identify possible network formation in solution, DOSY NMR measurements were performed in deuterated chloroform for 1:1 mixtures (L:R) of the resorcinarenes **1** and **2** and the bivalent halogen bond donating linkers **A**–**C**. The average diffusion coefficients obtained for the linker-resorcinarene mixtures (5.82-6.08x10⁻¹⁰ m²s⁻¹), however, did not differ notably from the diffusion coefficients of the pure resorcinarene solutions (5.93-5.94x10⁻¹⁰ m²s⁻¹, Table S3). This indicates that in solution stable larger structures are not formed even though halogen bonds are present. This is most likely caused by the more complex and competing interactions prevailing in solution compared to the solid state. In addition, the complex dynamic behavior of C-methyl resorcinarene skeleton shown in variable temperature NMR could prevent the optimal preorganization of the resorcinarene framework and self-assembly into larger network in solution.

Conclusions

Tetramethoxy resorcinarene derivatives with 3- (**1**) and 4-pyridine (**2**) podand arms were synthesized in order to use them as tetravalent halogen bond acceptors to construct multidimensional network structures with monovalent bromo- and iodopentafluorobenzene (**D**-**E**) and bivalent *para*- and *meta*-substituted dibromo- and diiodotetrafluorobenzene (**A**-**C**) halogen bond donors in the solid state and in solution. In the solid state, multidimensional halogen bonded networks with a potential to porosity were successfully crystallized with the strongest halogen bond forming 1,4-diiodotetrafluorobenzene linker **B**. 3-Pyridyl functionalized resorcinarene **1** assembled into a linear chain structure, whereas, interlocked tangled grid structure was obtained with the 4-pyridyl substituted resorcinarene **2**, with enantiomeric separation of the left and right handed resorcinarene isomers. The halogen bonds expand 2-dimensionally but the multidimensionality of the structures are achieved by the 3-D structure of the resorcinarene.

The halogen bond formation between the resorcinarenes and all of the halogen bond donors was also observed in solution by NMR spectroscopic studies, but the formation of larger networks was not observed, likely due to complex dynamics of the resorcinarene core and competing multiple interactions. The number of donor sites (mono vs bivalent linkers) and the position of the donor atom (*para*- vs. *meta*-substitution) were all observed to affect the halogen bond formation in solution either as a downfield shift (monovalent and *meta*-substituted linkers) or as an upfield shift (bivalent *para*-substituted linkers) in the linker ^{19}F NMR signals. DFT calculations of respective model systems supported the observed relationship between the direction of the chemical shift and binding mode. The combination of DFT calculations

and experimental methods is thus a convenient tool for predicting and interpreting halogen bonding in solution, which is still poorly understood phenomenon with larger building blocks.

Pyridine functionalized resorcinarenes **1** and **2** with preorganized structural features of the core and podand arms have proven to be an inspiring example of how predefined 3D macrocyclic structures can be exploited in the design and construction of multilevel nanosized halogen bond networks with a potential to porosity.

Experimental

General ^{1}H, ^{13}C, ^{19}F, COSY, HMQC and HMBC NMR spectra were recorded on a Bruker Avance DRX 500 MHz spectrometer and DOSY measurements on a Bruker Avance DRX 400 MHz spectrometer. Accurate ESI mass spectra were measured with a Micromass LCT ESI-TOF instrument. Melting points were obtained with a Stuart melting point apparatus SMP3. Tetramethoxy resorcinarene was prepared according to a literature procedure.[19] All other reagents were commercial and used as received. Detailed synthetic procedures and characterizations are provided in ESI.

3-Pyridyl Functionalized Resorcinarene Tetrapodand 1. A mixture of tetramethoxy resorcinarene[19] (0.25 g, 0.42 mmol) and Cs_2CO_3 (1.13 g, 3.47 mmol) in dry DMF (20 ml) at 90 °C

(bath temperature) was stirred for 60 min under nitrogen before the dropwise addition of 3-(chloromethyl)pyridine hydrochloride (0.31 g, 1.88 mmol) in DMF (10 ml). The dark brown suspension was stirred at 90 °C for 21 hours, after which it was filtered through a pad of Hyflo Super®. Solvent was evaporated under reduced pressure and the residue was dissolved in dichloromethane (70 ml). The organic layer was washed once with deionized water (70 ml) and once with brine (70 ml) before drying it with $MgSO_4$. Solvent was evaporated under reduced pressure. Recrystallization of the residue from a methanol-chloroform solution afforded an off-white powder (yield 0.19 g, 47%); m.p. 257-260 °C; ^{1}H NMR (500 MHz, $CDCl_3$, -30 °C): δ 1.45 (d, $^3J_{HH}$=6.75 Hz, 6H; CH_3), 1.54 (d, $^3J_{HH}$=6.70 Hz, 6H; CH_3), 3.21 (s, 6H; OCH_3), 3.68 (s, 6H; OCH_3), 4.16 (d, $^2J_{HH}$=10.30 Hz, 2H; CH_2), 4.49 (q, $^3J_{HH}$=6.89 Hz, 2H; CH), 4.70 (q, $^3J_{HH}$=6.89 Hz, 2H; CH), 4.78 (d, $^2J_{HH}$=10.40 Hz, 2H; CH_2), 5.36 (AB q, $^2J_{HH}$=11.00 Hz, 4H; CH_2), 5.99 (s, 2H; ArH), 6.21 (s, 2H; ArH), 6.57 (s, 2H; ArH), 6.77 (d, $^3J_{HH}$=7.60 Hz, 2H; PyH), 6.92 (q, $^3J_{HH}$=4.13 Hz, 2H; PyH), 7.35 (s, 2H; ArH), 7.39 (q, $^3J_{HH}$=4.15 Hz, 2H; PyH), 7.96 (d, $^3J_{HH}$=7.80 Hz, 2H; PyH), 8.20 (s, 2H; PyH), 8.48 (d, $^3J_{HH}$=4.00 Hz, 2H; PyH), 8.61 (d, $^3J_{HH}$=4.00 Hz, 2H; PyH), 8.85 ppm (s, 2H; PyH); ^{13}C NMR (126 MHz, $CDCl_3$, -30 °C): δ 19.6 (CH_3), 19.8 (CH_3), 30.8 (CH), 55.1 (OCH_3), 55.4 (OCH_3), 67.6 (CH_2), 68.2 (CH_2), 95.2 (ArC), 96.4 (ArC), 123.2 (PyC), 123.9 (PyC), 124.7 (ArC), 124.8 (ArC), 125.1 (ArC), 128.7 (ArC), 129.2

Table 1 Crystal data and structure refinement details.

	2-MeCN	**2**-CHCl$_3$	**1**-MeOH	**2**-EtOH	**1**-B	**2**-B
Formula	$C_{60}H_{60}N_4O_8 \cdot$ CHCl$_3$ $\cdot$ 2 MeCN	$C_{60}H_{60}N_4O_8 \cdot$ 3 CDCl$_3$	$C_{60}H_{60}N_4O_8 \cdot$ 3 CH$_3$OH	$C_{60}H_{60}N_4O_8 \cdot$ CHCl$_3$ $\cdot$ CH$_3$CH$_2$OH	$C_{60}H_{60}N_4O_8 \cdot$ 1.5 C$_6$F$_4$I$_2$ $\cdot$ CDCl$_3$	0.5 $C_{60}H_{60}N_4O_8 \cdot$ C$_6$F$_4$I$_2$ $\cdot$ CHCl$_3$
Formula weight	1166.60	1326.24	1061.25	1130.56	1688.28	1003.79
Crystal system	Triclinic	Triclinic	Triclinic	Monoclinic	Triclinic	Orthorhombic
Space group	P-1	P-1	P-1	P2$_1$/n	P-1	Pccn
a (Å)	13.4640(6)	13.5142(6)	13.4616(2)	13.1236(4)	13.0454(3)	11.07141(13)
b (Å)	13.6873(6)	14.6744(7)	14.1115(3)	32.8276(8)	13.7948(5)	44.2970(7)
c (Å)	17.0771(6)	17.3471(7)	15.8347(4)	13.3088(4)	20.6219(7)	15.7761(4)
α (°)	107.657(4)	95.199(4)	109.783(2)	90	88.043(3)	90
β (°)	95.015(3)	94.142(3)	96.6810(16)	92.373(3)	82.996(2)	90
γ (°)	95.481(3)	110.327(4)	99.7937(16)	90	84.693(2)	90
V (Å^3)	2962.5(2)	3192.8(2)	2765.07(10)	5728.7(3)	3666.6(2)	7737.1(2)
Formula units in unit cell, Z	2	2	2	4	2	8
D_c (Mg m^{-3})	1.308	1.380	1.275	1.311	1.529	1.723
μ (mm^{-1})	0.216 (Mo Kα)	0.451 (Mo Kα)	0.705 (Cu Kα)	0.221 (Mo Kα)	1.457 (Mo Kα)	1.894 (Mo Kα)
$F(000)$	1228	1372	1132	2384	1674	3936
Theta range for data collection (°)	4.1 to 53.4	1.90 to 30.54	3.36 to 74.33	1.99 to 26.70	1.96 to 26.70	1.84 to 30.64
Reflections collected	23583	31473	19429	27084	30106	66831
Independent reflections	12529 [R(int)=0.0358]	17184 [R(int)=0.0450]	10886 [R(int)=0.0255]	12119 [R(int)=0.0379]	15519 [R(int)=0.0298]	11090 [R(int)=0.0459]
Restrains/parameters	0/758	8/776	0/717	3/723	0/855	0/473
Goodness of fit on F^2	1.026	1.040	1.021	1.035	1.027	1.117
R_1 and R_2 [$I > 2\sigma(I)$]	0.0794, 0.2113	0.0997, 0.2724	0.0526, 0.1444	0.0815, 0.2186	0.0397, 0.0877	0.0486, 0.0974
R_1 and R_2 (all data)	0.1178, 0.2483	0.1889, 0.3400	0.0593, 0.1524	0.1307, 0.2609	0.0532, 0.0935	0.0700, 0.1054
Extinction coefficient	-	0.0043(11)	-	-	-	-
Largest difference peak and hole (e Å^{-3})	0.68, -0.98	0.653, -0.815	0.705, -0.495	0.537, -0.714	0.716, -0.876	0.554, -0.695

(ArC), 132.2 (PyC), 133.4 (PyC), 135.1 (PyC), 136.2 (PyC), 148.5 (PyC), 148.7 (PyC), 149.2 (PyC), 153.5 (ArC), 154.7 (ArC), 155.1 (ArC), 155.5 ppm (ArC); HRMS (ESI-TOF): m/z calcd for $C_{60}H_{60}O_8N_4 + H^+$: 965.4484 [M + H]$^+$; found 965.4495.

4-Pyridyl Functionalized Resorcinarene Tetrapodand 2. A mixture of tetramethoxy resorcinarene[19] (0.25 g, 0.42 mmol) and Cs_2CO_3 (1.18 g, 3.62 mmol) in dry DMF (20 ml) at 90 °C (bath temperature) was stirred for 60 min under nitrogen before the dropwise addition of 4-(chloromethyl)pyridine hydrochloride (0.31 g, 1.88 mmol) in DMF (10 ml). The brown suspension was stirred at 90 °C for 22 hours, after which it was filtered through a pad of Hyflo Super®. Solvent was evaporated under reduced pressure. The residue was dissolved in dichloromethane (50 ml) and it was washed twice with brine (2×50 ml). The organic layer was then dried over $MgSO_4$. Solvent was evaporated under reduced pressure and the residue was recrystallized from a methanol-chloroform solution affording an off-white crystalline solid (yield 0.20 g, 49%); m.p. 277-280 °C; ^1H NMR (500 MHz, CDCl$_3$, -30 °C): δ 1.47 (d, $^3J_{HH}$=6.75 Hz, 6H; CH$_3$), 1.57 (d, $^3J_{HH}$=6.75 Hz, 6H; CH$_3$), 3.16 (s, 6H; OCH$_3$), 3.72 (s, 6H; OCH$_3$), 4.30 (d, $^2J_{HH}$=11.80 Hz, 2H; CH$_2$), 4.52 (q, $^3J_{HH}$=7.00 Hz, 2H; CH), 4.70-4.74 (d+q, 4H; CH$_2$+CH), 5.31 (s, 4H; CH$_2$), 5.98 (s, 2H; ArH), 6.15 (s, 2H; ArH), 6.47 (s, 2H; ArH), 6.70 (d, $^3J_{HH}$=5.20 Hz, 4H; PyH), 7.36 (s, 2H; ArH), 7.54 (d, $^3J_{HH}$=5.45 Hz, 4H; PyH), 8.33 (d, $^3J_{HH}$=5.35 Hz, 4H; PyH), 8.66 ppm (d, $^3J_{HH}$=5.70 Hz, 4H; PyH); ^{13}C NMR (126 MHz, CDCl$_3$, -30 °C): δ 19.5 (CH$_3$), 19.7 (CH$_3$), 31.0 (CH), 55.3 (OCH$_3$), 55.4 (OCH$_3$), 68.0 (CH$_2$), 68.4 (CH$_2$), 94.8 (ArC), 96.0 (ArC), 121.3 (PyC), 121.9 (PyC), 124.6 (ArC), 125.0 (ArC), 126.3 (ArC), 128.5 (ArC), 129.0 (ArC), 145.8 (PyC), 147.0 (PyC), 149.3 (PyC), 150.0 (PyC), 153.3 (ArC), 154.7 (ArC), 155.6 ppm (ArC); HRMS (ESI-TOF): m/z calcd for $C_{60}H_{60}O_8N_4 + H^+$: 965.4484 [M + H]$^+$; found 965.4465.

Benzyl Functionalized Resorcinarene Tetrapodand 3. A white suspension of tetramethoxy resorcinarene[19] (0.25 g, 0.42 mmol), benzyl bromide (210 µl, 1.77 mmol), dibenzo-18-crown-6 (0.04 g, 0.12 mmol) and Cs_2CO_3 (0.98 g, 2.99 mmol) was refluxed in acetonitrile (30 ml) under nitrogen for 24 h. The warm reaction mixture was filtered by suction through a pad of Hyflo Super®. Chloroform was filtered through the same pad of Hyflo Super® in case the product had crystallized during filtration. The solvents were then evaporated under vacuum and the resulting off-white residue was dissolved in chloroform (50 ml). The organic layer was washed once with deionized water (50 ml) and once with brine (50 ml) after which it was dried over $MgSO_4$. The solvent was evaporated to dryness under vacuum. The product was recrystallized twice from a methanol-chloroform solution. Yield: 0.34 g (85%) of white crystalline solid; m.p. 235-236 °C; ^1H NMR (500 MHz, CDCl$_3$, -30 °C): δ 1.46 (d, $^3J_{HH}$=6.40 Hz, 6H; CH$_3$), 1.57 (d, $^3J_{HH}$=6.40 Hz, 6H; CH$_3$), 3.17 (s, 6H; OCH$_3$), 3.63 (s, 6H; OCH$_3$), 4.23 (d, $^2J_{HH}$=10.00 Hz, 2H; CH$_2$), 4.53 (q, $^3J_{HH}$=6.80 Hz, 2H; CH), 4.71 (d, $^2J_{HH}$=10.00 Hz, 2H; CH$_2$), 4.78 (q, $^3J_{HH}$=6.80 Hz, 2H; CH), 5.34 (AB q, $^2J_{HH}$=7.70 Hz, 4H; CH$_2$), 6.03 (s, 2H; ArH), 6.20 (s, 2H; ArH), 6.58 (s, 2H; ArH), 6.70 (d, $^3J_{HH}$=7.85 Hz, 4H; BnH), 7.03 (t, $^3J_{HH}$=7.83 Hz, 4H; BnH), 7.18 (t, $^3J_{HH}$=7.15 Hz, 2H; BnH), 7.36-7.40 (s+t, 4H; ArH+BnH), 7.46 (t, $^3J_{HH}$=7.25 Hz, 4H; BnH),

7.65 ppm (d, $^3J_{HH}$=7.40 Hz, 4H; PyH); ^{13}C NMR (126 MHz, CDCl$_3$, -30 °C): δ 19.7 (CH$_3$), 19.9 (CH$_3$), 30.7 (CH), 30.9 (CH), 55.1 (OCH$_3$), 55.4 (OCH$_3$), 69.9 (CH$_2$), 70.5 (CH$_2$), 95.5 (ArC), 96.0 (ArC), 124.3 (ArC), 124.7 (ArC), 125.8 (BnC), 126.9 (BnC), 127.6 (BnC), 127.8 (BnC), 127.9 (BnC), 128.0 (ArC), 128.7 (ArC), 128.9 (ArC), 129.0 (ArC), 136.4 (BnC), 138.1 (BnC), 153.7 (ArC), 154.7 (ArC), 155.3 (ArC), 155.6 ppm (ArC); HRMS (ESI-TOF): m/z calcd for $C_{64}H_{64}O_8 + Na^+$: 983.4493 [M + Na]$^+$; found 983.4476.

X-Ray crystallography. The data were recorded with AGILENT SuperNova diffractometer using a micro-focus X-ray source and multilayer optics monochromatized MoK$_α$ [λ(MoK$_α$) = 0.71073 Å; 50 kV, 0.8 mA] radiation (**2**-MeCN, **2**-CHCl$_3$, **2**-EtOH, **1**-**B** and **2**-**B**) or CuK$_α$ [λ(CuK$_α$) = 1.54178 Å; 50 kV, 0.8 mA] radiation (**1**-MeOH). Data for the structure **1**-MeOH was collected at 120 K, for structure **2**-EtOH at 173 K and for structures **2**-MeCN, **2**-CHCl$_3$, **1**-**B** and **2**-**B** at 170 K. The data were processed using Crysalis^{PRO} [29] and analytical absorption correction was made according to Clark and Reid.[30] The structures were solved by direct methods (SHELXS-97[31]) or by charge flipping (Superflip[32]) integrated in the Olex2 program[33]. The refinements, based on F^2, were made by full-matrix least-squares techniques (SHELXL-97[31]). All hydrogen atoms were calculated to their idealized positions with isotropic temperature factors (1.2 or 1.5 times the C temperature factor) and refined as riding atoms. CCDC numbers 1044954 (**2**-MeCN), 1044955 (**2**-CHCl$_3$), 1044956 (**1**-MeOH), 1044957 (**2**-EtOH), 1044958 (**1**-**B**) and 1044959 (**2**-**B**) contain the crystallographic data for this paper.

DFT computations. NMR-shifts were calculated using Gauge-Including Projector-Augmented Wave (GIPAW) formalism as implemented in pseudopotential and planewave based DFT-code Quantum Espresso.[34] Before calculation of NMR-shifts the structures were relaxed to the energy minimum configuration until all components of the forces of all atoms were at maximum 0.026 eV/Å. For calculations we used ultrasoft PBE pseudopotentials, kinetic energy cutoff of 820 eV for wavefunctions and kinetic energy cutoff of 8200 eV for the charge density and potential. An energy convergence criterion for the self-consistency was set to $1.4 \cdot 10^{-11}$ eV. All the results for total chemical shifts were reported related to the linker molecule for which the ^{19}F NMR-shift was set to zero.

Acknowledgements

Notes and references

1 G. R. Desiraju, P. Ho, L. Kloo, A. C. Legon, R. Marquardt, P. Metrangolo, P. Polizer, G. Resnati and K. Rissanen, *Pure Appl. Chem.*, 2013, **85**, 1711–1713.

2 For a review see (a) P. Metrangolo, F. Meyer, T. Pilati, G. Resnati and G. Terraneo, *Angew. Chem. Int. Ed.,* 2008, **47**, 6114–6127; (b) P. Metrangolo, G. Resnati, *Cryst. Growth Des.,* 2012, **12**, 5835–5838; (c) A. Priimagi and G. Cavallo, *Acc. Chem. Res.*, 2013, **46**, 2686–2695.

3 (a) S. M. Huber, J. D. Scanlon, E. Jimenez-Izal, J. M. Ugalde and I. Infante, *Phys. Chem. Chem. Phys.,* 2013, **15**, 10350–10357; (b) A. C. Legon, *Phys. Chem. Chem. Phys.,* 2010, **12**, 7736–7747.

4 See for example (a) M. L. Mercuri, M. Atzori, A. Serpe, P. Deplano and J. A. Schlueter, *Inorg. Chem. Front.,* 2015, **2**, 108–115; (b) X. Pang, X. R. Zhao, H. Wang, H.-L. Sun and W. J. Jin, *Cryst. Growth Des.,* 2013, **13**, 3739–3745; (c) M. Fourmigué, in *Halogen bonding Fundamentals and Applications*, Vol. 126 (Eds. P. Metrangolo, G. Resnati), Structure and Bonding; Springer Berlin Heidelberg, 2008, pp. 181–207.

5 See for example (a) D. Bruce, in *Halogen bonding Fundamentals and Applications*, Vol. 126 (Eds. P. Metrangolo, G. Resnati), Structure and Bonding; Springer Berlin Heidelberg, 2008, pp. 161–180; (b) P. Metrangolo, C. Prasang, G. Resnati, R. Liantonio, A. C. Whitwood and D. W. Bruce, *Chem. Commun.,* 2006, 3290–3292; (c) H. L. Nguyen, P. N. Horton, M. B. Hursthouse, A. C. Legon and D. W. Bruce, *J. Am. Chem. Soc.,* 2003, **126**, 16–17.

6 See for example (a) D. Cincić, T. Friscić and W. Jones, *Chem. - A Eur. J.,* 2008, **14**, 747–753; (b) A. De Santis, A. Forni, R. Liantonio, P. Metrangolo, T. Pilati and G. Resnati, *Chem. - A Eur. J.* 2003, **9**, 3974–3983; (c) E. Corradi, S. V Meille, M. T. Messina, P. Metrangolo and G. Resnati, *Angew. Chem. Int. Ed.,* 2000, **112**, 1852–1856.

7 (a) P. Metrangolo, F. Meyer, T. Pilati, D. M. Proserpio and G. Resnati, *Chem. - A Eur. J.,* 2007, **13**, 5765–5772; (b) R. Bertani, F. Chaux, M. Gleria, P. Metrangolo, R. Milani, T. Pilati, G. Resnati, M. Sansotera and A. Venzo, *Inorganica Chim. Acta,* 2007, **360**, 1191–1199; (c) M. Vartanian and A. Lucassen, *Cryst. Growth Des.,* 2008, **8**, 786–790; (d) M. Baldrighi, P. Metrangolo, F. Meyer, T. Pilati, D. Proserpio, G. Resnati and G. Terraneo, *J. Fluor. Chem.,* 2010, **131**, 1218–1224; (e) F. C. Pigge, P. P. Kapadia and D. C. Swenson, *CrystEngComm,* 2013, **15**, 4386–4391.

8 J.-L. Syssa-Magalé, K. Boubekeur, J. Leroy, L.-M. Chamoreau, C. Fave and B. Schöllhorn, *CrystEngComm,* 2014, **16**, 10380–10384.

9 (a) K. Raatikainen, J. Huuskonen, M. Lahtinen, P. Metrangolo and K. Rissanen, *Chem. Commun.,* 2009, 2160–2162; (b) K. Raatikainen and K. Rissanen, *Cryst. Growth Des.,* 2010, **10**, 3638–3646.

10 M. F. Geer, J. Mazzuca, M. D. Smith and L. S. Shimizu, *CrystEngComm,* 2013, **15**, 9923–9929.

11 For a quick review see (a) W. Sliwa, C. Kozlowski in *Calixarenes and Resorcinarenes*, WILEY-VCH, Weinheim, 2009; (b) P. Timmerman, W. Verboom and D. N. Reinhoudt, *Tetrahedron,* 1996, **52**, 2663–2704.

12 See for example (a) A. Vargas Jentzsch, D. Emery, J. Mareda, P. Metrangolo, G. Resnati and S. Matile, *Angew. Chem. Int. Ed.,* 2011, **50**, 11675–11678; (b) N. K. Beyeh, M. Cetina and K. Rissanen, *Chem. Commun.,* 2014, **50**, 1959–1961; (c) C. L. D. Gibb, E. D. Stevens and B. C. Gibb, *J. Am. Chem. Soc.,* 2001, **123**, 5849–5850; (d) G. Wagner, W. Knoll, M. M. Bobek, L. Brecker, H. W. G. van Herwijnen and U. H. Brinker, *Org. Lett.*, 2009, **12**, 332–335; (e) N. K. Beyeh, D. P. Weimann, L. Kaufmann, C. A. Schalley and K. Rissanen, *Chem. – A Eur. J.,* 2012, **18**, 5552–5557.

13 (a) M. T. Messina, P. Metrangolo, S. Pappalardo, M. F. Parisi, T. Pilati and G. Resnati, *Chem. - A Eur. J.,* 2000, **6**, 3495–3500; (b) C. B. Aakeröy, A. Rajbanshi, P. Metrangolo, G. Resnati, M. F. Parisi, J. Desper and T. Pilati, *CrystEngComm,* 2012, **14**, 6366–6368; (c) L. Turunen, N. K. Beyeh, F. Pan, A. Valkonen and K. Rissanen, *Chem. Commun.,* 2014, **50**, 15920–15923.

14 (a) B.-Q. Ma and P. Coppens, *Cryst. Growth Des.,* 2004, **4**, 211–213; (b) B.-Q. Ma and P. Coppens, *Cryst. Growth Des.,* 2004, **4**, 1377–1385; (c) B.-Q. Ma, L. F. V. Ferreira and P. Coppens, *Org. Lett.,* 2004, **6**, 1087–1090; (d) C. L. Barnes and E. Bosch, *Cryst. Growth Des.,* 2005, **5**, 1049–1053; (e) J. M. Matheny, E. Bosch and C. L. Barnes, *Cryst. Growth Des.,* 2007, **7**, 984–988; (f) C. L. Barnes and E. Bosch, *J. Chem. Crystallogr.,* 2007, **37**, 783–786; (g) R. S. Patil, A. V Mossine, H. Kumari, C. L. Barnes and J. L. Atwood, *Cryst. Growth Des.*, 2014, **14**, 5212–5218.

15 (a) M. Erdélyi, *Chem. Soc. Rev.,* 2012, **41**, 3547–3557; (b) T. M. Beale, M. G. Chudzinski, M. G. Sarwar and M. S. Taylor, *Chem. Soc. Rev.,* 2013, **42**, 1667–1680.

16 See for example (a) M. T. Messina, P. Metrangolo, W. Panzeri, E. Ragg and G. Resnati, *Tetrahedron Lett.,* 1998, **39**, 9069–9072; (b) P. Metrangolo, W. Panzeri, F. Recupero and G. Resnati, *J. Fluorine Chem.*, 2002, **114**, 27–33; (c) R. Cabot and C. A. Hunter, *Chem. Commun.,* 2009, 2005–2007; (d) M. Sarwar, B. Dragisic, L. L. Salsberg, C. Gouliaras and M. S. Taylor, *J. Am. Chem. Soc.,* 2010, **132**, 1646–1653; (e) D. Hauchecorne, B. J. van der Veken and P. E. Hansen, *Chem. Phys.*, 2011, **381**, 5-10; (f) B. Hawthorne, H. Fan-Hagenstein, E. Wood, J. Smith and T. Hanks, *Int. J. Spectrosc.,* 2013, Article ID 216518, 10 pages.

17 S. H. Jungbauer, D. Bul, F. Kniep, C. W. Lehmann, E. Herdtweck and S. M. Huber, *J. Am. Chem. Soc.,* 2014, **136**, 16740–16743.

18 T.-R Tero, K. Salorinne and M. Nissinen, *CrystEngComm,* 2012, **14**, 7360–7367.

19 T.-R. Tero, A. Suhonen, K. Salorinne, H. Campos-Barbosa and M. Nissinen, *Org. Lett.,* 2013, **15**, 1096–1099.

20 K. Helttunen, K. Salorinne, T. Barboza, H. C. Barbosa, A. Suhonen and M. Nissinen, *New J. Chem.,* 2012, **36**, 789–795.

CrystEngComm Accepted Manuscript

Please do not adjust margins
CrystEngComm

Journal Name

ARTICLE

21 M. J. McIldowie, M. Mocerino, M. I. Ogden and B. W. Skelton, *Tetrahedron,* 2007, **63**, 10817–10825.

22 L. Abis, E. Dalcanale, A. Du Vosel and S. Spera, *J. Chem. Soc. Perkin Trans. 2,* 1990, 2075–2080.

23 Synthetized according to M. Luostarinen, K. Salorinne, H. Lähteenmäki, H. Mansikkamäki, C. A. Schalley, M. Nissinen and K. Rissanen, *J. Incl. Phenom. Macrocycl. Chem.,* 2007, **58**, 71–80.

24 B.-Q. Ma and P. Coppens, *Chem. Commun.,* 2002, 424–425.

25 (a) B.-Q. Ma, Y. Zhang and P. Coppens, *CrystEngComm,* 2001, **3**, 78–80; (b) B.-Q. Ma, Y. Zhang and P. Coppens, *Cryst. Growth Des.,* 2001, **2**, 7–13.

26 M. He, R. J. Johnson, J. O. Escobedo, P. A. Beck, K. K. Kim, N. N. St. Luce, C. J. Davis, P. T. Lewis, F. R. Fronczek, B. J. Melancon, A. A. Mrse, W. D. Treleaven and R. M. Strongin, *J. Am. Chem. Soc.,* 2002, **124**, 5000–5009.

27 M. J. McIldowie, M. Mocerino, B. W. Skelton and A. H. White, *Org. Lett.*, 2000, **2**, 3869–3871.

28 K. Salorinne and M. Nissinen, *CrystEngComm*, 2009, **11**, 1572–1578.

29 CrysAlisPro, Agilent Technologies, Version 1.171.36.21 (release 14-08-2012 CrysAlis171.NET)

30 R. C. Clark and J. C. Reid, *Acta Crystallogr. Sect. A,* 1995, **51**, 887-897.

31 G. M. Sheldrick, *Acta Crystallogr. Sect. A,* 2008, **64**, 112–122.

32 (a) L. Palatinus and G. Chapuis, *J. Appl. Crystallogr.,* 2007, **40**, 786–790; (b) L. Palatinus and A. van der Lee, *J. Appl. Crystallogr.,* 2008, **41**, 975–984; (c) L. Palatinus, S. J. Prathapa and S. van Smaalen, *J. Appl. Crystallogr.,* 2012, **45**, 575–580.

33 O. V. Dolomanov, L. J. Bourhis, R. J. Gildea, J. A. K. Howard and H. Puschmann, *J. Appl. Crystallogr.,* 2009, **42**, 339–341.

34 P. Giannozzi, S. Baroni, N. Bonini, M. Calandra, R. Car, C. Cavazzoni, D. Ceresoli, G. L. Chiarotti, M. Cococcioni, I. Dabo, A. Dal Corso, S. de Gironcoli, S. Fabris, G. Fratesi, R. Gebauer, U. Gerstmann, C. Gougoussis, A. Kokalj, M. Lazzeri, L. Martin-Samos, N. Marzari, F. Mauri, R. Mazzarello, S. Paolini, A. Pasquarello, L. Paulatto, C. Sbraccia, S. Scandolo, Gabriele Sclauzero, Ari P. Seitsonen, Alexander Smogunov, Paolo Umari and Renata M. Wentzcovitch, *J.Phys.: Condens. Matter*, 2009, **21**, 395502.

Table of Content

In the solid state, pyridine functionalized resorcinarenes formed multidimensional networks with aryl halides. The solution behavior of these XB systems was analyzed by combining NMR spectroscopy and DFT computations.